

# ME699 Stage-2 report

P. Vachan Deep  
Roll # 184104002  
November 15, 2019

---

## 1 Introduction

The blood circulation system is one of the most complicated and important systems essential for proper body functioning. The nature of blood flow shows significant differences in a body with diseases, especially cardiac ailments. For example, areas with low wall shear stress areas in an artery are likely to cause plaque (cholesterol, lipids and other material) deposition which can have fatal effects. Blood flow visualisation has, therefore, been of interest for medical purposes.

About five decades back, the only observation possible was mere flow rate measurement. This was performed by physical probing of certain arteries in unconscious animals. As time progressed, for ethical reasons and also due to availability of better visualisation techniques, such measurements were abolished. Currently, blood flow measurement using MRI is prevalent. In this technique, the patient is injected with a contrast that reacts to magnetic field before exposition to the MRI machine.

## 2 Objectives

There are two aims of this work.

1. By how much does a realistic magnetic field effect blood flow nature in the aortic arch.
2. How does magnetic field change the flow characteristics of a fluid (not necessarily blood) through the aortic arch geometry.

## 3 Methods and simulation setup

### 3.1 Geometry

The geometry considered is a simplification of aortic arch: the very first artery that is connected directly to the heart. The diameter of aorta is assumed constant with value 2 cm. The shape of the aorta is obtained by sweeping this cross-section for 10 cm of the ascending portion, followed by the aortic semi-circular arch of radius 4 cm opening into a 5 cm descending portion. The geometry is shown in Fig. 1.

### 3.2 Modelling

Compelled by the need to perform a simulation, many physical characteristics of blood and its flow in arteries are not considered in this work.

1. Blood is modelled as a Newtonian fluid. In reality, blood is a suspension of particles in fluid which definitely has non-Newtonian behaviour.
2. The conductivity of blood is assumed constant. In reality, the concentration of red blood cells (which may not be distributed uniformly) affects the conductivity.
3. The arteries are either considered insulated or perfectly conducting while they have finite conductivity in reality.
4. The arteries are assumed rigid. In reality, the arteries are flexible to such an extent that wave propagation phenomenon were reported in blood flow which is otherwise incompressible and involves no waves.

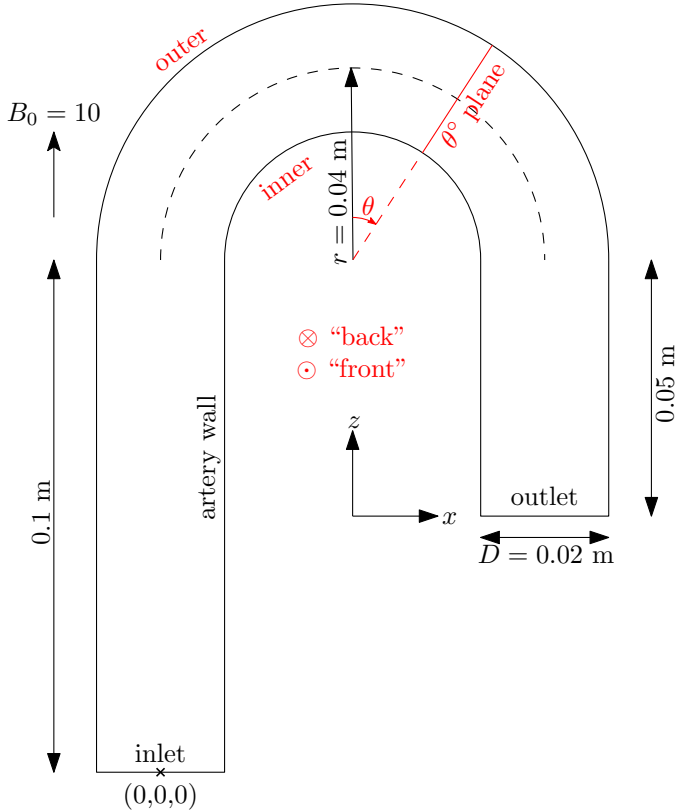


**Figure 1:** Geometry of aorta considered for this study.

5. The flow is assumed laminar. However, during the systolic phase, the Reynold's number can be as high as 4000 which can actually induce transition.

The average density of blood is reported to be  $1060 \text{ kg/m}^3$  [1]. The kinematic viscosity is found to be about  $3 \times 10^{-6} \text{ m}^2/\text{s}$  [2]. The conductivity of blood as a function of the hematocrit—the volume percentage of red blood cells in blood—is presented by HIRSCH *et al.* [3]. The average hematocrit is reported to be between 40 and 50 percent [4] based on which, the conductivity can be deduced to be about 0.5 mho/m [3]. The inlet velocity is prescribed to have a sinusoidal variation with a frequency of 1 Hz (60 beats per minute):  $u(t) = 0.25 + 0.15 \sin(2\pi t)$

The boundary conditions at the inlet, outlet and artery wall are now described.

- Inlet

$$\mathbf{u} = [0.25 + 0.15 \sin(2\pi t)]\mathbf{e}_z \quad \frac{\partial p}{\partial n} = 0 \quad \frac{\partial \mathbf{B}}{\partial n} = \mathbf{0}$$

- Outlet

$$\frac{\partial \mathbf{u}}{\partial n} = \mathbf{0} \quad p = 0 \quad \frac{\partial \mathbf{B}}{\partial n} = \mathbf{0}$$

- Artery wall

$$\mathbf{u} = \mathbf{0} \quad \frac{\partial p}{\partial n} = 0 \quad \frac{\partial \mathbf{B}}{\partial n} = \mathbf{0} \text{ or } \mathbf{B} = 10 \mathbf{e}_z$$

At  $t = 0$  the velocity and pressure fields are initialised to zero, while the magnetic field is initialised to the imposed value.

The results for plain (without magnetic field) flow were obtained using pimpleFoam, an incompressible transient solver based on a combination of PISO and SIMPLE algorithms. The MHD flow results were obtained using mhdFoam. Both these solvers are part of the OpenFOAM software [5].

### 3.3 Cases

A total of five simulations including one plain simulation were performed. The four MHD simulations arise from combination of two conductivity values (0.5 mho/m and 50 mho/m) and two artery boundary conditions (insulating and perfectly conducting) considered. The two cases involving higher conductivity are not representations of blood flow but of a different fluid.

### 3.4 Mesh

The mesh used for all simulations is shown in Fig. 2. It is a simple extrusion of a 2D mesh along the artery centreline. This mesh, generated using Gmsh [6], has about 2 million cells.

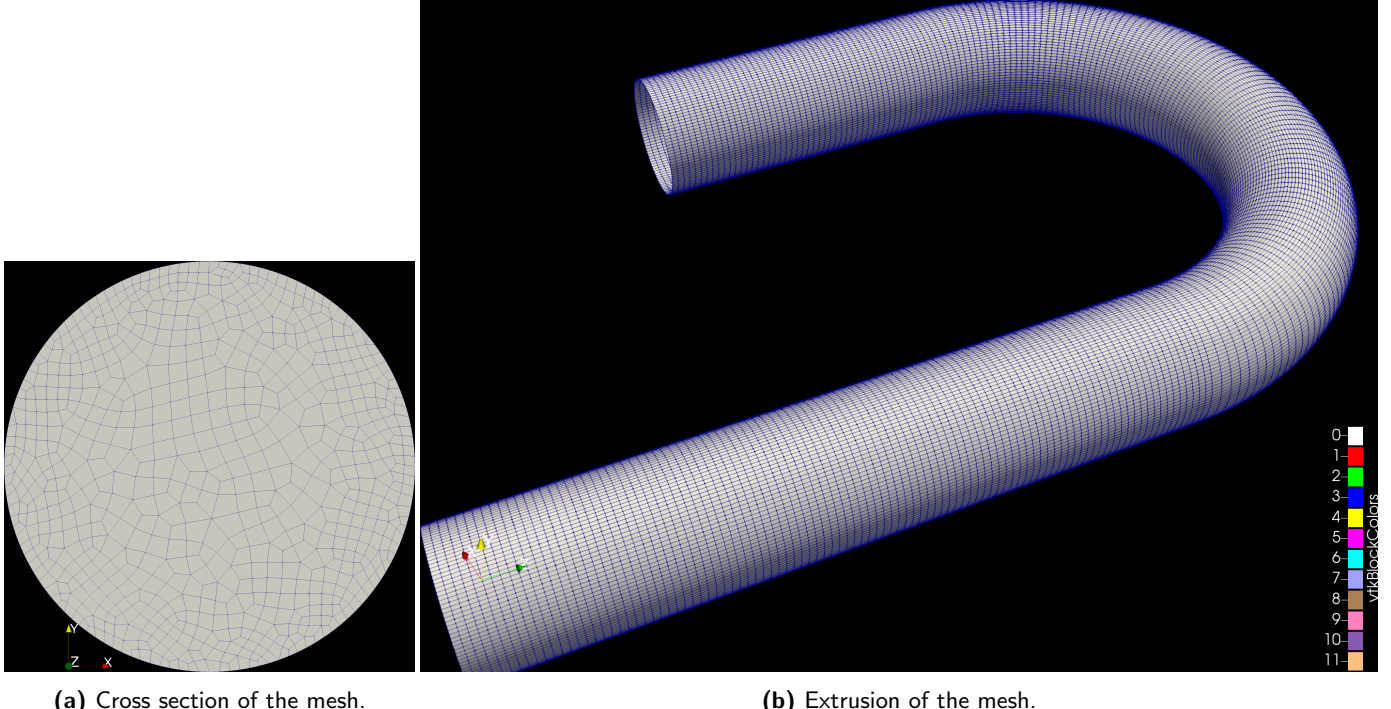


**Figure 2:** The mesh considered for this work.

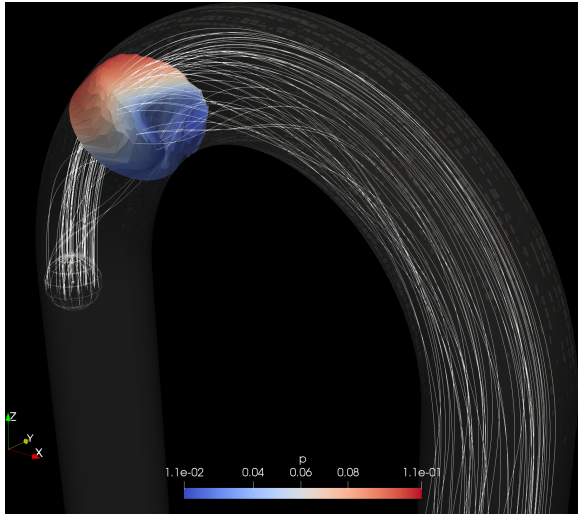
## 4 Results

### 4.1 Plain flow

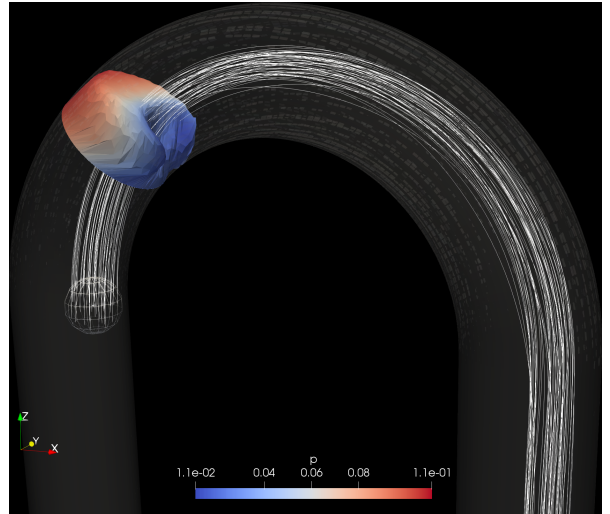
Some terminology will now be introduced. All text in red in Fig. 1 will now be described. The inner curvature of artery is called “inner” and the outer curvature “outer”. Further, the +ve  $y$  direction is called “backward” and –ve  $y$  direction “front”. Any plane inclined at an angle  $\theta$  to the  $x$ -normal plane, cutting the artery will be called the “ $\theta^\circ$  plane” as shown in Fig. 1.

The streamlines of plain flow are shown in Fig. 3. Keep in mind that inlet velocity is maximum at  $n + 0.25$  s and minimum at  $n + 0.75$  s where  $n$  is an integer. From Figs. 3a and 3b, it can be concluded that the inner fluid particles try to avoid the high pressure region at the inner part of the arch by gradually moving to the outer region. At the same time, the front and back (not shown) streamlines try to move to the inner region, and gain some vorticity in this process thus generating a double-helical streamline pattern. It is possible that this is also responsible for the high velocity lobes seen on the inner side in Figs. 3a and 3b. It has been postulated that this double-helical streamline pattern helps in separation mitigation [7]. These helices function to supply high velocity fluid from the core to the inner region where velocity is low and/or points upstream.

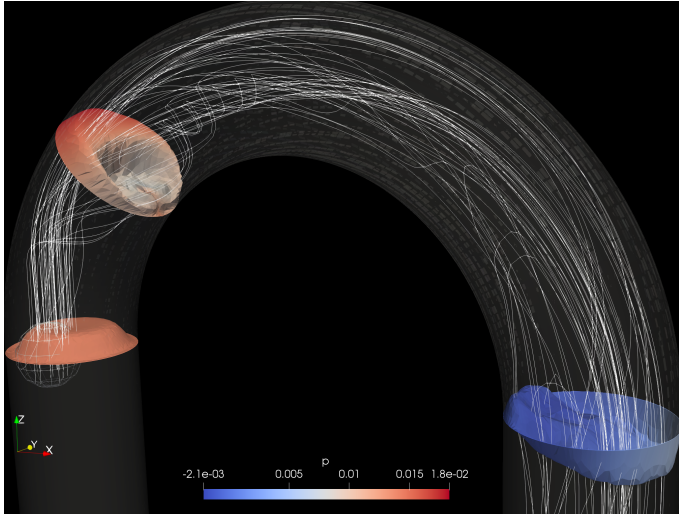
Back flow starts in the aorta at 1.5 s near the beginning of descending portion and then propagates up to the



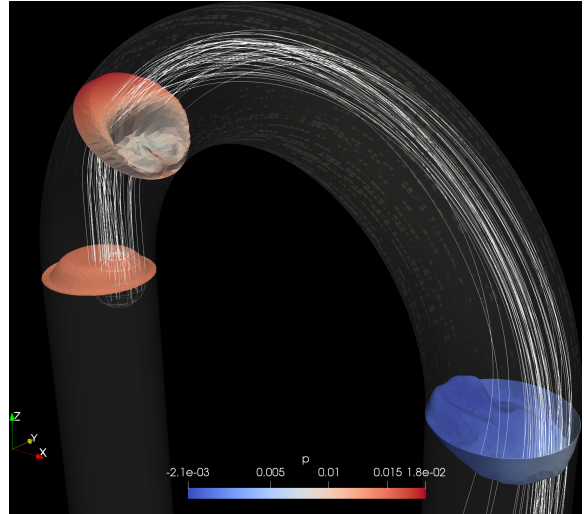
(a) Streamlines generated from front source at 1.25 s.



(b) Streamlines generated from inner source at 1.25 s.



(c) Streamlines generated from front source at 1.75 s.



(d) Streamlines generated from inner source at 1.75 s.

**Figure 3:** Streamlines at different time instants (1.25 s and 1.75 s) with different sources. All the sources are 50 particles distributed in a sphere of radius 0.5 cm (half the artery radius). The centre of sphere is at (0,-0.5,0) cm for front sources and at (0.5,0,0) cm for inner sources. The 3D surfaces in this figures are generated by deforming  $0^\circ$ ,  $\pm 45^\circ$  planes with the local fluid velocity. Colour represents pressure.

$0^\circ$  plane by 1.75 s, as shown in Fig. 4. In fact, as will be seen in Subsection 4.2, at 1.75 s, a significant part of inner portion has back flow.

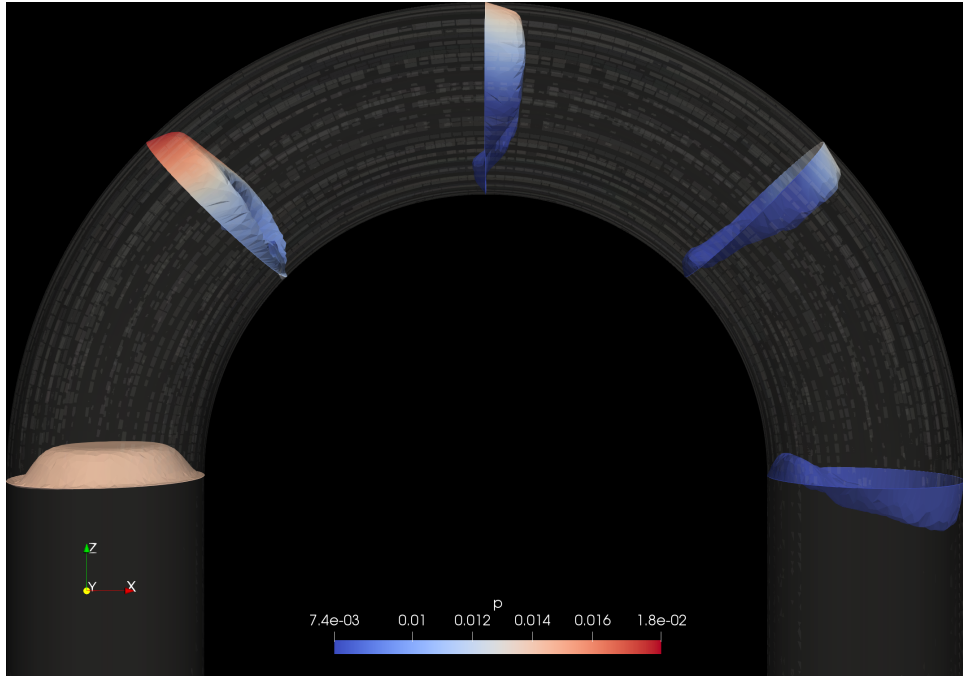


**Figure 4:**  $0^\circ$ ,  $\pm 45^\circ$  and  $\pm 90^\circ$  planes deformed with local fluid velocity. Notice the back flow in  $0^\circ$ ,  $45^\circ$  and  $90^\circ$  planes. Colour represents pressure.

## 4.2 Low conductivity MHD flow

Here, the conductivity of the fluid is taken 0.5 mho/m which actually approximates the blood's conductivity. Taking characteristic length  $l = 0.1$  m (length of ascending portion), the magnetic Reynold's number  $Re_m \sim 10^{-8}$ . Taking  $l = 0.01$  m (radius of aorta) for estimating viscous forces, the Hartmann number  $Ha \sim 1$ . Using the unsteady term for inertial force estimate, the interaction parameter  $N \sim 0.05$ . It can therefore be expected that magnetic field will not have much affect on blood flow. In fact, Fig. 5 shows that even at 1.75 s where one can expect maximum differences between plain and MHD flow, the velocity vectors match almost perfectly.

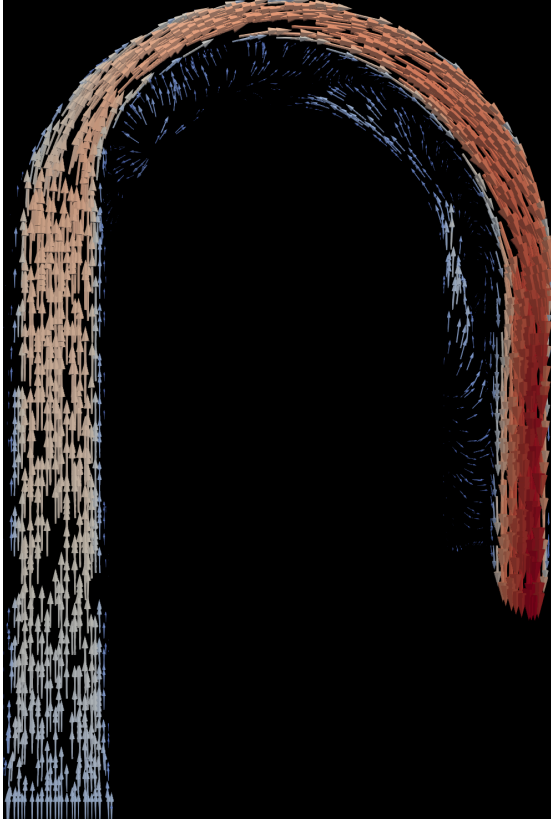
One can however, inspect current patterns in the MHD case, and their variation with wall boundary condition. Fig. 6 shows the current patterns with insulating wall for  $\pm 45^\circ$ ,  $0^\circ$  planes at 1.25 s and 1.75 s. At the centre where the velocity is highest, the current  $\mathbf{J}$  points in the direction of  $\mathbf{u} \times \mathbf{B}$  and then curls along the insulating artery walls to ensure zero divergence. Also note the minor current circulations in the inner region where high velocity lobes are observed. Fig. 7 shows current patterns on the same planes at 0.75 s. Notice that now the current is uni-directional.

Comparing Figs. 6 and 7, one could conclude that due to the direction of current on inner side, the Lorentz force points downstream and upstream due to insulating and perfectly conducting wall respectively. It might therefore be expected that while an insulating wall can suppress separation, a perfectly conducting wall might support separation. However, this conclusion will be proven false in Subsection 4.3.

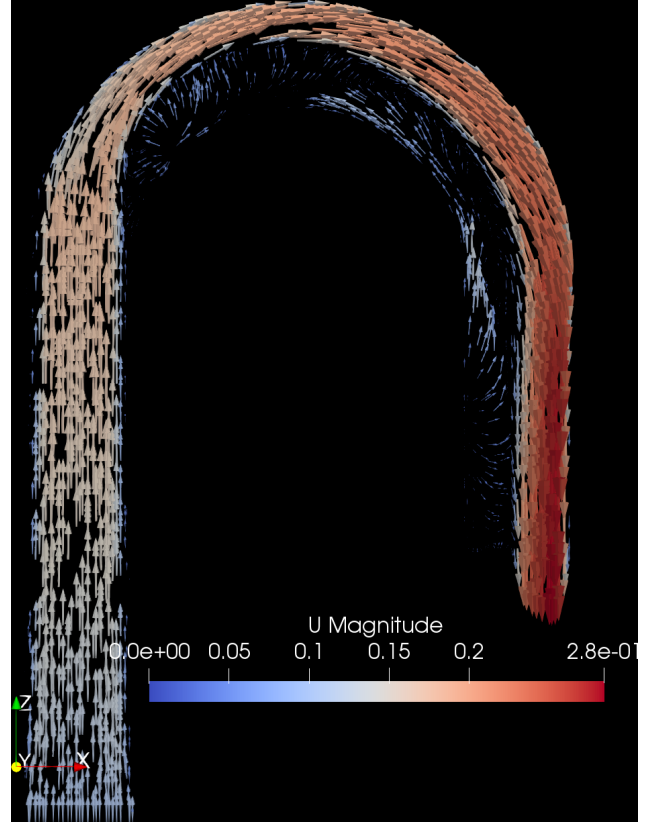
## 4.3 High conductivity MHD flow

Here, the conductivity of the fluid is taken 0.5 mho/m, 100 times the value considered in Subsection 4.2. The non-dimensional numbers now scale accordingly as  $Re_m \sim 10^{-6}$ ,  $Ha \sim 10$  and  $N \sim 5$ . The current patterns in this case are similar to low conductivity case as can be seen from Fig. 8. The comparison of velocity vectors on  $y = 0$  for this case is shown in Fig. 9 for both wall boundary conditions.

It is un-expected to see that separation has reduced even with perfectly conducting wall in which, the current direction make Lorentz force act in upstream direction. In fact, perfectly conducting wall case counters separation, to some extent, even in the descending portion where negligible current is induced as  $\mathbf{u}$  is anti-parallel to  $\mathbf{B}$ . The



(a) Plain flow.



(b) Low conductivity MHD flow with insulating artery wall boundary condition.

**Figure 5:** Velocity vectors on  $y = 0$  plane. Notice the apparent lack of any differences.

explanation to this observation is based on flow helicity ( $h$ ) which is defined as  $h = \mathbf{u} \cdot \boldsymbol{\omega} = \mathbf{u} \cdot (\nabla \times \mathbf{u})$ . It has been mentioned in Subsection 4.1 how helical nature of streamlines helps in reducing separation. Shown in Fig. 10 is the comparison of helicity between all the three cases at 1.75 s. Among all, the perfectly conducting wall has the highest helicity magnitude. Because the helical nature has been increased, the flow is able to have lesser separation, even though Lorentz force supports separation.

For the two types of wall boundary conditions, Lorentz force exhibits two different mechanisms to reduce separation. With an insulated wall, the force itself points upstream thereby opposing back flow. With a perfectly conducting wall, the Lorentz force generates helicity which allows the flow to mitigate separation. Further, this might be the explanation to the observation made in previous paragraph: why a perfectly conducting wall suppresses back flow even in the descending portion. Because the Lorentz force has generated more helicity, the flow itself is more capable of reducing separation, without any assistance from Lorentz force. This mechanism is not active in the insulating wall case since Lorentz force decreases magnitude of helicity in this case (Fig. 10b).

## 5 Conclusion

This study begun with a question on the validity of MRI based visualisation techniques for blood flow: does the blood flow remain minimally disturbed by the magnetic field? This was the first question. It became clear immediately from Fig. 5 that the answer to this question is yes. However, it is worth recalling the assumptions made in Subsection 3.2. At least, few of these are so critical that relaxing them might change the nature of flow completely. To comprehend the complexity involved, transitional flow of corpuscular fluid in flexible artery walls is so difficult to model that it involves three very actively researched areas in fluid dynamics: transition, multi-phase flow and fluid-structure interaction. It is not very obvious that the realistic value of magnetic field considered here (10 T) will not affect blood flow in any way, like in Fig. 5.

A second question then arose: how does a flow in this geometry get affected by magnetic field. To answer this, two different simulations for two different wall boundary conditions were done with fluid properties set to give reasonable

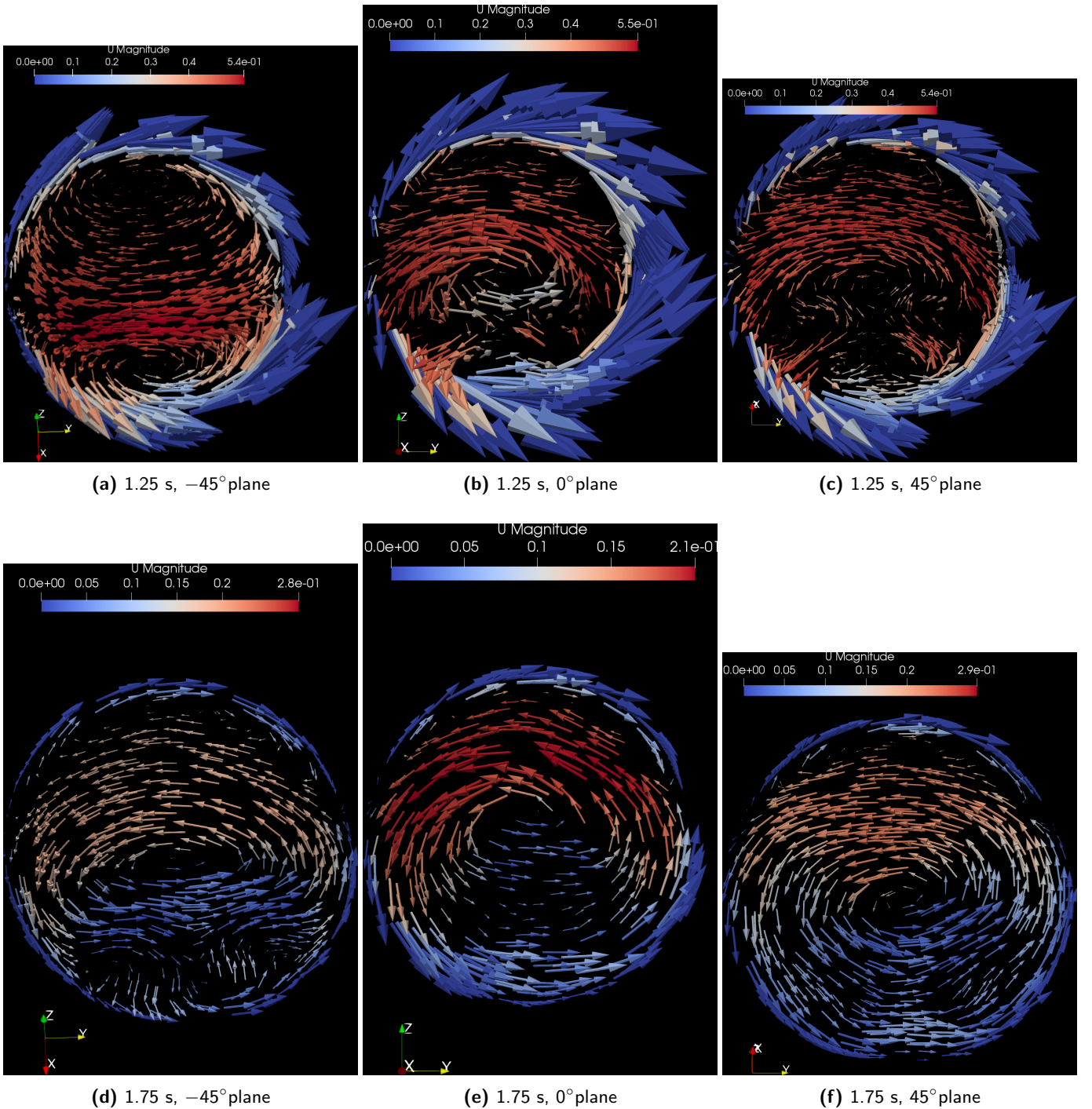


**Figure 6:** Current density patterns at different planes and time instants. All plots are with insulating wall boundary condition. The direction and magnitude of arrows represents  $\mathbf{J}$ , while the colour represents  $||\mathbf{u}||$ .

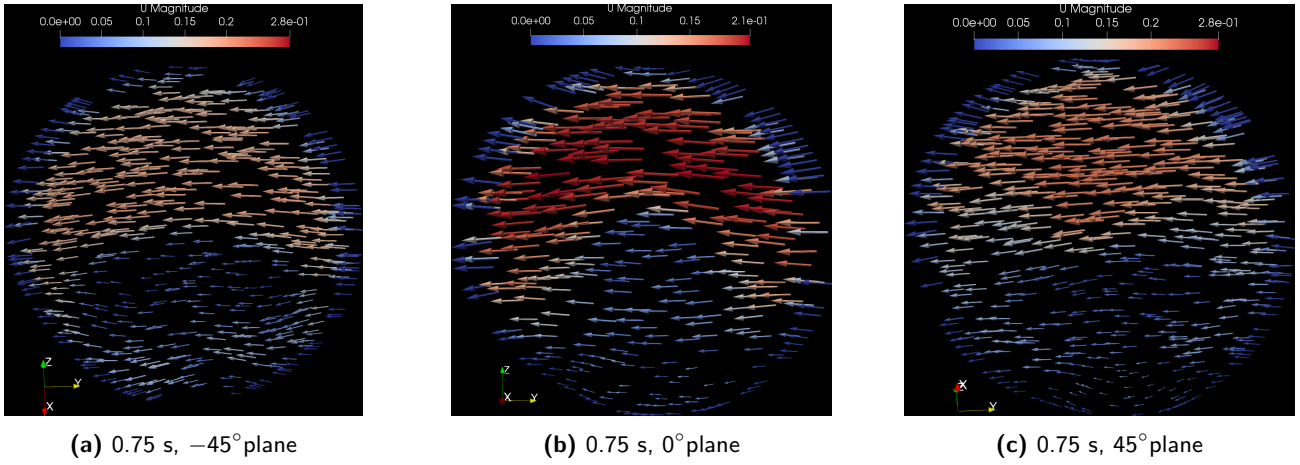


**Figure 7:** Current density patterns at different planes and time instants. All plots are with perfectly conducting wall boundary condition. The direction and magnitude of arrows represents  $\mathbf{J}$ , while the colour represents  $\|\mathbf{u}\|$ .

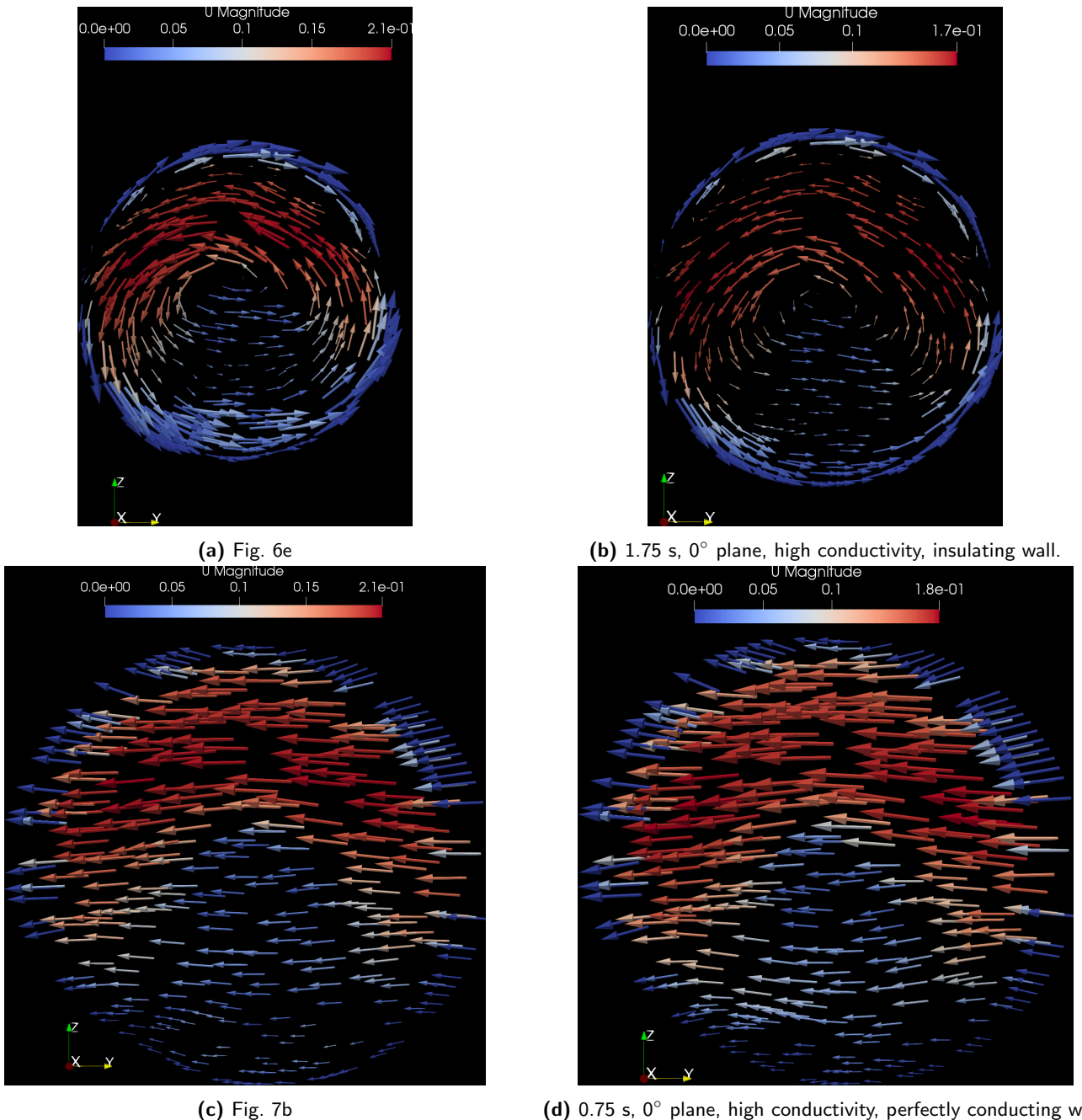
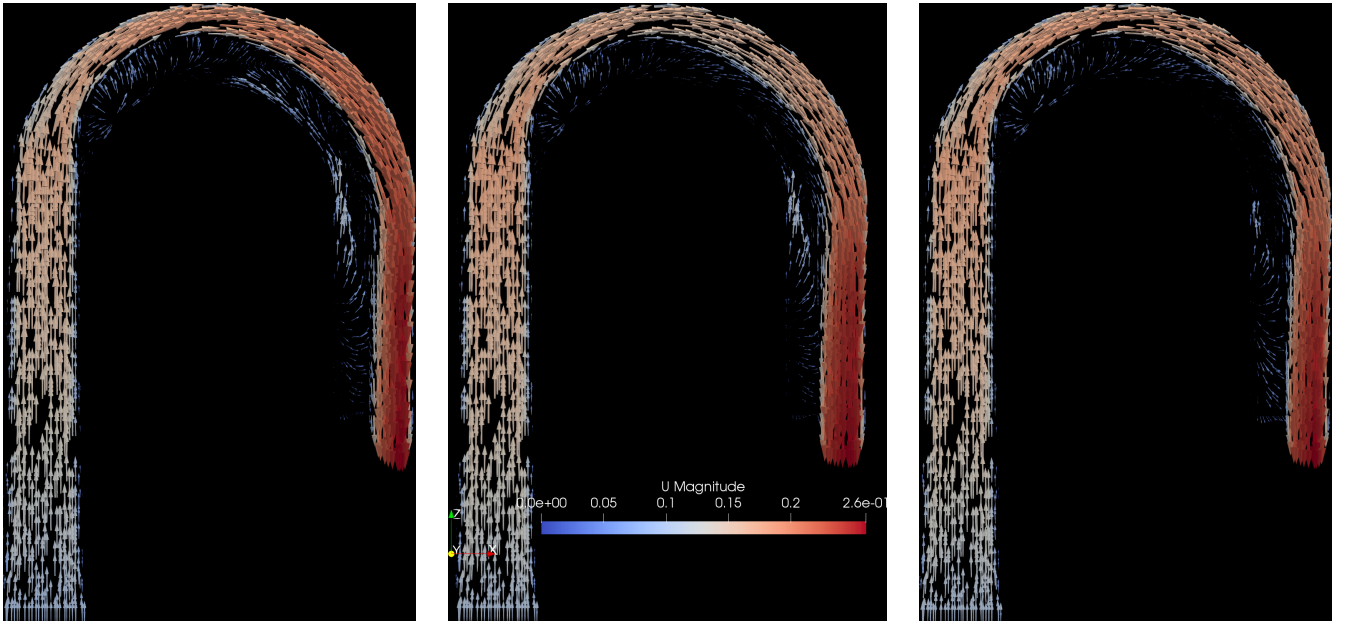


**Figure 8:** Comparison of current patterns between low and high conductivity cases. The direction and magnitude of arrows represents  $\mathbf{J}$ , while the colour represents  $\|\mathbf{u}\|$ . The current vectors in (b) and (d) have scales different from Figs. 6e and 7b.

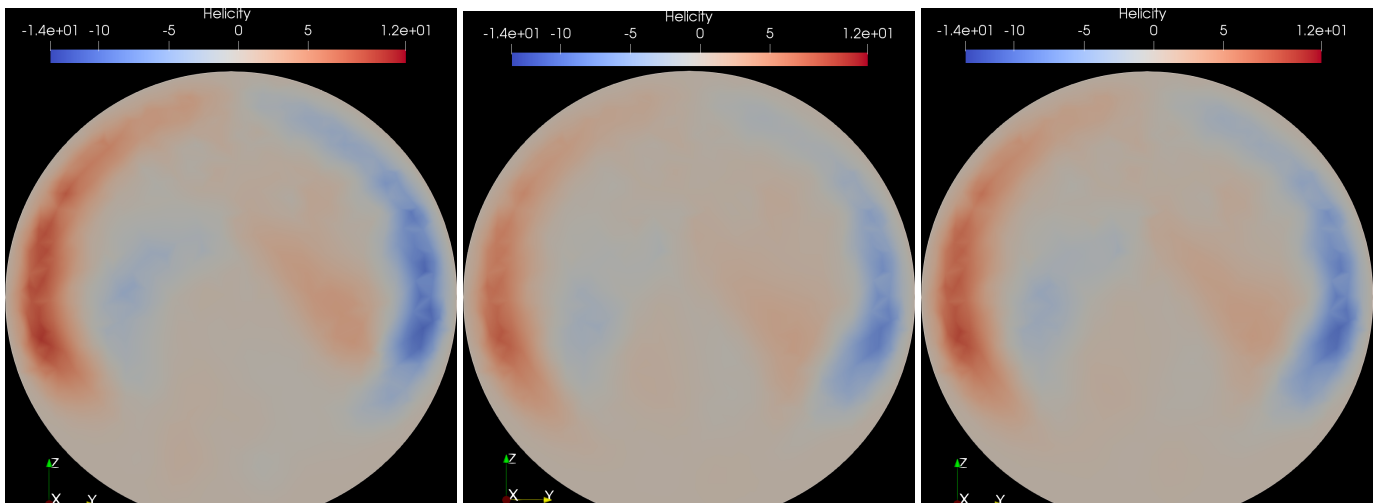


(a) Fig. 5a.

(b) High conductivity MHD flow with insulating artery wall boundary condition.

(c) High conductivity MHD flow with perfectly conducting wall boundary condition.

**Figure 9:** Velocity vectors on  $y = 0$  plane.



(a) 1.75 s, plain flow.

(b) 1.75 s, high conductivity MHD flow, insulating wall.

(c) 1.75 s, high conductivity MHD flow, perfectly conducting wall.

**Figure 10:** Comparison of helicity at  $0^\circ$  plane at 1.75 s. Notice the increase in magnitude of helicity in perfectly conducting wall case compared to insulated wall case. Although not clearly visible, the range of helicity is widest for the perfectly conducting wall case. The plain flow helicity ranges approximately from  $-10$  to  $10$ , and the insulating wall helicity ranges approximately from  $-8$  to  $8$ .

values of  $\text{Ha}$  and  $N$ . The most significant observation here is the exhibition of two different mechanisms by which Lorentz force suppresses separation. As has been detailed in Subsection 4.3, the Lorentz force points upstream in the insulating wall case to suppress separation, while it generates helicity in the perfectly conducting wall case which in return reduces separation. The suppression of helicity in insulating wall case was also mentioned. These two cases exemplify vorticity suppression and generation mechanisms of the Lorentz force.

It might be challenging and interesting to investigate the mechanism of helicity generation. A simple probable explanation will now be presented. This hypothesis will only be “first order” in the sense that assuming velocity and vorticity fields from plain flow case, current field from MHD flow cases, comments on helicity rise/decline will be made. Of course, such compartmentalisation does not depict the actually physics because of the two way coupling between magnetic and velocity fields. In this context, the analysis presented here will only be the “first iteration” and many such iterations combined will actually capture the flow physics. Nevertheless proceeding, the momentum and vorticity equations are

$$\frac{\partial \mathbf{u}}{\partial t} + \boldsymbol{\omega} \times \mathbf{u} = -\nabla \left( \frac{p}{\rho} + \frac{u^2}{2} \right) + \nu \nabla^2 \mathbf{u} + \frac{1}{\rho} \mathbf{J} \times \mathbf{B}_0, \quad (1)$$

$$\frac{\partial \boldsymbol{\omega}}{\partial t} + \mathbf{u} \cdot \nabla \boldsymbol{\omega} = \boldsymbol{\omega} \cdot \nabla \mathbf{u} + \nu \nabla^2 \boldsymbol{\omega} + \frac{1}{\rho} \nabla \times (\mathbf{J} \times \mathbf{B}_0). \quad (2)$$

Taking dot products of Eqs. (1) and (2) with  $\boldsymbol{\omega}$  and  $\mathbf{u}$  respectively, and adding, one gets Eq. (3), an evolution equation for helicity, of which the Lorentz force term ( $S$ ) is of interest.

$$\frac{Dh}{Dt} = \dots + \underbrace{\frac{1}{\rho} [(\mathbf{J} \times \mathbf{B}_0) \cdot \boldsymbol{\omega} + \mathbf{u} \cdot [\nabla \times (\mathbf{J} \times \mathbf{B}_0)]]}_{S} \quad (3)$$

Since  $\mathbf{B}_0$  is invariant in space,  $S$  can be simplified. Also, it has been observed that only the in-plane<sup>1</sup> components of  $\mathbf{J}$  are significant, meaning, its component parallel to  $\mathbf{u}$  is negligible.

$$S = (\mathbf{J} \times \mathbf{B}_0) \cdot \boldsymbol{\omega} + B_0 \frac{\partial \mathbf{J}}{\partial z} \cdot \mathbf{u} \approx (\mathbf{J} \times \mathbf{B}_0) \cdot \boldsymbol{\omega} \quad (4)$$

Now, taking near-wall region in interest, vorticity can be assumed to predominantly have two components: the azimuthal component due to velocity boundary layer and and axial component due to helical streamlines. Since  $\mathbf{J}$  is in-plane, the azimuthal component does not contribute to  $S$ . Consider the back ( $+y$  side) portion in Fig. 10 for analysis where  $\mathbf{u}$  is in  $x$  direction and vorticity due to helical flow is in  $-x$  direction, with  $\mathbf{B}$  in  $+z$  direction. From Fig. 8b (insulating wall), it can be seen that  $\mathbf{J} \times \mathbf{B}$  points in  $+x$  direction, both above and below the centreline, making  $S$  negative. The opposite is the story for perfectly conducting wall for which Fig. 8d shows that  $\mathbf{J} \times \mathbf{B}$  points in  $-x$  direction, making  $S$  positive. It is thus argued that helicity increases for perfectly conducting wall and decreases for insulated wall. Similar arguments can be sought for the front ( $-y$ ) portion. Overall, this analysis shows that helicity magnitude is enhanced by a perfectly conducting wall and reduced by an insulating wall.

Note that the above analysis is too simple. All terms other than the Lorentz force term have been ignored in Eq. (3). These ignored terms involve vorticity, velocity and pressure which also change when a magnetic field is applied and behave differently for different walls. Further, since it was known from Fig. 10 that most of helicity generation occurs at the front and back side walls, only these regions were analysed. Lastly, the out-of-plane component of  $\mathbf{J}$  was ignored which is a valid assumption so long as the in-plane velocity components do not dominate.

## References

- Shmukler, M. *Density Of Blood* [Online; accessed 12-September-2019]. 2004. <https://hypertextbook.com/facts/2004/MichaelShmukler.shtml>.
- Wikipedia contributors. *Hemorheology — Wikipedia, The Free Encyclopedia* [Online; accessed 12-September-2019]. 2019. <https://en.wikipedia.org/w/index.php?title=Hemorheology&oldid=915252588>.

<sup>1</sup>As in, lying on a  $\theta^\circ$  plane without significant out-of-plane component.

3. HIRSCH, F. G., TEXTER, E. C., WOOD, L. A., BALLARD, W. C., HORAN, F. E., WRIGHT, I. S., FREY, C. & STARR, D. THE ELECTRICAL CONDUCTIVITY OF BLOOD. *Blood* **5**, 1017–1035. ISSN: 0006-4971. eprint: <http://www.bloodjournal.org/content/5/11/1017.full.pdf>. <http://www.bloodjournal.org/content/5/11/1017> (1950).
4. Wikipedia contributors. *Hematocrit — Wikipedia, The Free Encyclopedia* [Online; accessed 12-September-2019]. 2019. <https://en.wikipedia.org/w/index.php?title=Hematocrit&oldid=912296822>.
5. The OpenFOAM Foundation. *OpenFOAM* 2019. <https://openfoam.org/>.
6. Geuzaine, C. & Remacle, J.-F. Gmsh: A 3-D finite element mesh generator with built-in pre-and post-processing facilities. *International journal for numerical methods in engineering* **79**, 1309–1331 (2009).
7. Morbiducci, U., Ponzini, R., Rizzo, G., Cadioli, M., Esposito, A., Montevercchi, F. M. & Redaelli, A. Mechanistic insight into the physiological relevance of helical blood flow in the human aorta: an in vivo study. *Biomechanics and modeling in mechanobiology* **10**, 339–355 (2011).